

# Complex Cytochrome P450 Kinetics Due to Multisubstrate Binding and Sequential Metabolism. Part 1. Theoretical Considerations<sup>1</sup>

Zeyuan Wang,<sup>1</sup> Erickson M. Paragas,<sup>1</sup> Swati Nagar, and Ken Korzekwa

*Department of Pharmaceutical Sciences, Temple University School of Pharmacy, Philadelphia, Pennsylvania*

Received May 25, 2021; accepted September 06, 2021

## ABSTRACT

Complexities in P450-mediated metabolism kinetics include multi-substrate binding, multiple-product formation, and sequential metabolism. Saturation curves and intrinsic clearances were simulated for single-substrate and multisubstrate models using derived velocity equations and numerical solutions of ordinary differential equations (ODEs). Multisubstrate models focused on sigmoidal kinetics because of their dramatic impact on clearance predictions. These models were combined with multiple-product formation and sequential metabolism, and simulations were performed with random error. Use of single-substrate models to characterize multisubstrate data can result in inaccurate kinetic parameters and poor clearance

predictions. Comparing results for use of standard velocity equations with ODEs clearly shows that ODEs are more versatile and provide better parameter estimates. It would be difficult to derive concentration-velocity relationships for complex models, but these relationships can be easily modeled using numerical methods and ODEs.

## SIGNIFICANCE STATEMENT

The impact of multisubstrate binding, multiple-product formation, and sequential metabolism on the P450 kinetics was investigated. Numerical methods are capable of characterizing complicated P450 kinetics.

## Introduction

Drug metabolism plays an important role in determining the pharmacokinetic and pharmacodynamic properties of drug candidates. Cytochrome P450s (P450s) are a superfamily of enzymes involved in the metabolism of over 70% of drugs currently on the market (Zanger and Schwab, 2013). P450-mediated clearance and related drug interactions can be a major issue during drug development. P450s demonstrate unusual kinetics with respect to ligand selectivity (Ekroos and Sjögren, 2006) and multiple-substrate binding. In many cases, multisubstrate binding results in atypical saturation kinetics, including sigmoidal saturation, substrate inhibition, and biphasic saturation curves (Korzekwa et al., 1998; Tracy, 2006). Spectral binding and X-ray crystallography studies support the theory that the active sites of some P450s are large and flexible (Shou et al., 1994; Ueng et al., 1997; Korzekwa et al., 1998; Hosea et al., 2000; Domanski et al., 2001; Ekins et al., 2003; Yoon et al., 2004) and can accommodate the simultaneous binding of multiple substrates (Li and Poulos, 2004; Wester et al., 2005; Roberts et al., 2011; Nguyen et al., 2016; Sevrioukova and Poulos, 2017). In addition to the simultaneous multiple binding of molecules of the same substrate, binding of different substrates occurs as well, resulting in

heterotropic activation and inhibition (Ueng et al., 1997; Kenworthy et al., 2001; Hutzler and Tracy, 2002; Galetin et al., 2003; Collom et al., 2008; Blobaum et al., 2013). There are many possible factors that may be involved in non-Michaelis-Menten P450 kinetics, including active site flexibility, distinct binding sites (Hosea et al., 2000), and protein-protein interactions (Jamakhandi et al., 2007; Davydov et al., 2017; Dangi et al., 2021). However, most experimental saturation curves can be represented adequately by simpler enzyme-substrate complex (ES) and enzyme-substrate-substrate complex (ESS) models.

The combination of active site flexibility, fast rotation speed of substrate molecules in the active site, and versatile active oxygen species (Guengerich, 2018) results in multiple-metabolite formation in a parallel or sequential manner (Masubuchi et al., 1996; Galetin et al., 2004; Obach, 2013). Multiple primary metabolites formed from the ES and ESS complex (Jones and Korzekwa, 1996) and secondary metabolite formation (Pang, 1995) add more complexity to P450 kinetics. Velocity equations as a function of substrate concentration and initial conditions are not easily derived for these complex schemes.

Since Cleland published methods for the least-squares analysis of enzyme kinetic data in 1979 (Cleland, 1979), there has been a steady movement away from graphical methods for kinetic analyses to robust statistical analyses by model fitting to derived velocity equations (e.g., the Michaelis-Menten equation) and various methods of numerical analysis (Hemker, 1972; Plant, 1979; Frenzen and Maini, 1988; Johnson, 2009; Kuzmič, 2009; Manimozhi et al., 2010; Rajendran et al., 2018; Yadav et al., 2021). For enzyme kinetic models with one independent variable (time), kinetic schemes can be represented as a collection of ordinary differential equations (ODEs). In addition to the derivation and use of velocity equations to model enzyme kinetics, ODEs can be used with numerical

This work was supported by National Institutes of Health National Institute of General Medical Sciences (to K.K. and S.N.) [Grants 2R01GM104178 and 2R01GM114369].

The authors have no financial disclosures, and no conflicts of interest to report.

<sup>1</sup>Z.W. and E.M.P. contributed equally to the work.

[dx.doi.org/10.1124/dmd.121.000553](https://doi.org/10.1124/dmd.121.000553).

 This article has supplemental material available at [dmd.aspetjournals.org](http://dmd.aspetjournals.org).

**ABBREVIATIONS:**  $CL_{int}$ , intrinsic clearance; E, enzyme; ES, enzyme-substrate complex; ESS, enzyme-substrate-substrate complex; EP, enzyme-product complex;  $ES^*$ , active oxygenating species derived from ES;  $ESS^*$ , active oxygenating species derived from ESS; ESSP, one product formation from the ESS model; ESSP1P2, two product formation from the ESS model; ESP, one product formation from the ES model; ESP1P2, two product formation from the ES model;  $E_t$ , total enzyme concentration; k, rate constant;  $k_{cat}$ , catalytic turnover rate;  $K_m$ , Michaelis-Menten constant; ODE, ordinary differential equation; P, product; P450, cytochrome P450; S, substrate.

methods to directly model and parameterize complex kinetic schemes. The complex P450 kinetics encountered in time-dependent inactivation, including inactivator binding, inhibitor depletion, and sequential metabolism, have been previously modeled using numerical analysis (Korzekwa et al., 2014; Nagar et al., 2014; Yadav et al., 2018, 2020, 2021).

P450 kinetics parameters are often used to determine the enzymes responsible for metabolite formation and to predict the potential for drug-drug interactions. Another commonly used P450 assay measures substrate depletion over time to estimate the intrinsic clearance ( $CL_{int}$ ) of a reaction. This is the first-order rate constant observed at low substrate concentrations for most kinetic schemes. This clearance is then used to scale up to predict drug clearance in humans. It has been demonstrated that use of a different concentration range may lead to variable *in vitro*  $CL_{int}$  estimations when sigmoidal kinetics are observed (Komura et al., 2005; Iwaki et al., 2019). Simulations have shown that  $V_{max}/K_m$  will not be accurate when sigmoidal kinetics are observed and the turnover rate from the ES complex approaches zero (Korzekwa, 2021).

With respect to sequential metabolism and multiple metabolites, numerical solutions have been reported previously (Frenzen and Maini, 1988; Varón et al., 2005), but no derived velocity equations have been reported, possibly due to the complex branched pathways that must be considered. The numerical method is facile for modeling multiple-metabolite formation. Modeling metabolite exposure is a crucial issue in drug discovery and development especially for active (Obach, 2013) and toxic circulating metabolites (Schadt et al., 2018). Numerical analysis using ODEs is expected to easily provide accurate parameters for multiple metabolites, possibly leading to more accurate *in vivo* predictions of drug metabolism and metabolite disposition.

In part 1 of these manuscripts, we demonstrate the use of the numerical analyses in characterizing  $K_m$ ,  $V_{max}$ , and concentration-dependent  $CL_{int}$  upon multisubstrate binding, describing concentration-dependent metabolite ratios, and investigating sequential metabolism. In part 2, in-house data of three different model drugs—midazolam, ticlopidine and diazepam—were generated and analyzed with this modeling strategy.

## Materials and Methods

### Theoretical Considerations

Figure 1A shows the traditional single-substrate binding model, in which the EP complex is assumed to be short-lived compared with the ES complex. The equation derived from this scheme is the well known Michaelis-Menten equation

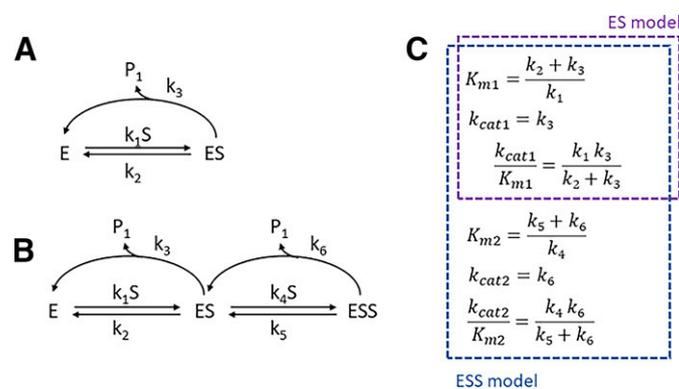


**Fig. 1.** Schemes for single-product formation. (A) A single-substrate binding (ES complex), one-metabolite formation (ESP) scheme is depicted. EP complex is not shown since fast product release is assumed. (B) A two-substrate binding (ESS complex), one-metabolite formation (ESSP) scheme is depicted. EP, ESP, and EPP are not shown since fast product release and no interaction between substrate and product within the active site are assumed. (C) Expressions for  $K_m$  and  $k_{cat}$  for schemes A (dashed purple box) and B (dashed blue box) are listed. Rate constants for all reactions are denoted by  $k_1$ – $k_6$ . The species depicted in the schemes are defined as follows: E, unbound enzyme; P1, product 1.

(Michaelis and Menten, 1913).

$$\frac{\text{velocity } (v)}{E_t} = \frac{V_{max}}{K_m + [S]} = \frac{k_{cat} [S]}{K_m + [S]} \quad (1)$$

in which  $k_{cat}$  is the maximum velocity at unit enzyme concentration ( $E_t$ ),  $[S]$  is the substrate concentration, and  $K_m$  is the substrate concentration at half-maximum turnover rate. Figure 1B shows a two-substrate model, which can result in non-Michaelis-Menten kinetics. Evidence of non-Michaelis-Menten (atypical) kinetics has been reported widely for many P450s, reactions, and substrates (Atkins, 2005, 2006). Multiple-substrate binding in the enzyme active site has been confirmed with X-ray crystallography (Yano et al., 2004; Gay et al., 2010). Most categories of atypical kinetics can be explained by Fig. 1B, wherein the specific binding orientation of substrates is not assumed. For these models, the first substrate binds to the enzyme active site with an apparent  $K_{m1} = (k_2 + k_3)/k_1$  and turnover rate  $k_{cat1} = k_3$ . A second substrate binds to the enzyme active site with an affinity  $K_{m2} = (k_5 + k_6)/k_4$  and turnover rate  $k_{cat2} = k_6$  (Fig. 1C). The  $K_m$  values are apparent since both processes occur simultaneously. Sigmoidal kinetics can be observed when  $K_{m1} > K_{m2}$  or  $k_{cat1} < k_{cat2}$ . Biphasic kinetics are observed when  $K_{m1} < K_{m2}$  and  $k_{cat1} < k_{cat2}$ . Substrate inhibition occurs at the condition of  $K_{m1} < K_{m2}$  and  $k_{cat1} > k_{cat2}$ .

Because of large and flexible binding pockets and nonspecific substrate orientation for some P450s (Shou et al., 1994; Ueng et al., 1997; Korzekwa et al., 1998; Hosea et al., 2000; Domanski et al., 2001; Ekins et al., 2003; Yoon et al., 2004), formation of multiple metabolites by a single P450 is common (Masubuchi et al., 1996; Galetin et al., 2004; Obach, 2013). Kinetic schemes that include the formation of two metabolites are shown in Fig. 2. The schemes in Fig. 2, A and B can correctly model the formation of two products when product formation is rate-limiting. However, for P450s, oxygen activation is rate-limiting, and substrate oxidation is fast (Luthra et al., 2011). The branch between formation of the two products occurs from the activated oxygen species and is not rate-limiting within the catalytic cycle (i.e., the branch is product determining but not rate-limiting). As described below, it is necessary to use the kinetic schemes in Fig. 2, C and D to describe multiproduct P450 kinetics. In these schemes,  $ES^*$  and  $ESS^*$  represent the activated oxygen species. It should be noted that  $K_{m1,P1} = K_{m1,P2}$ , and  $K_{m2,P1} = K_{m2,P2}$  is assumed since both products are formed from the same enzyme-substrate complex.

**Dataset Simulation.** Saturation curves (velocity vs. substrate concentration) were simulated as follows: 1) constructing ODEs for the kinetic schemes in Figs. 1 and 2, 2) varying either the dissociation or turnover rate constant, 3) simulating saturation curve data with or without adding random error, and 4) directly fitting the Michaelis-Menten equation, ESSP (one product formed from an ESS model) rate equation, and ODEs for the schemes in Figs. 1 and 2 to the simulated dataset and comparing the fitted parameters with those used in the simulation. Simulations were repeated 500 times, and the results were checked to determine convergence and the distribution of parameter estimates.

All association rate constants (e.g.,  $k_1$  and  $k_4$  in Fig. 1) were set to  $270 \mu\text{M}^{-1} \text{min}^{-1}$  (Barnaba et al., 2016). Simulated dissociation rate constants were selected to achieve the  $K_{m1}$  and  $K_{m2}$  values in the range of 1–1000  $\mu\text{M}$  (Walsky and Obach, 2004), and turnover rate constants ( $k_{cat1}$  and  $k_{cat2}$ ) were set within the range of 0–60  $\text{minute}^{-1}$ . The values were chosen to provide the desired saturation kinetic profiles (e.g., sigmoidal kinetics,  $[P2] > [P1]$ , etc.). For simulation of saturation curves, initial substrate concentrations were varied between 0 and 300  $\mu\text{M}$ ,  $E_t$  was 5 nM, and the incubation time was set at 5, 10, or 20 minutes. Substrate consumption in all saturation curve simulations was  $<10\%$  unless indicated.  $CL_{int}$  was simulated as the enzyme normalized value  $d[S]/(dt[S]E)$  over a range of 0.01–1  $\mu\text{M}$  initial substrate concentrations, with  $E_t = 100 \text{ nM}$ . Triplicate data with random error of substrate concentrations and incubation time were simulated from ESSP and ESSP1P2 (two products formed from an ESS model) ODEs, respectively. For some simulations and parameterizations, correlation between parameters is expected, and some parameters must be held constant. For example, if an enzyme species is not saturated within the range of substrate concentrations, both  $k_{cat}$  and  $K_m$  cannot be determined. One parameter must be held constant, and only the ratio of  $k_{cat}/K_m$  can be determined.

Simulated datasets were generated via the built-in function NDSolve in Mathematica 12.0 (Wolfram Research, Champaign, IL). Random errors were generated from RandomVariate and NormalDistribution function by setting the mean as one and relative standard deviation as 1%, 5%, 10%, and 20%. This error was multiplied by the simulated values to generate log-normally distributed values. For the simulations, 500 runs of triplicate data were generated at each error level.

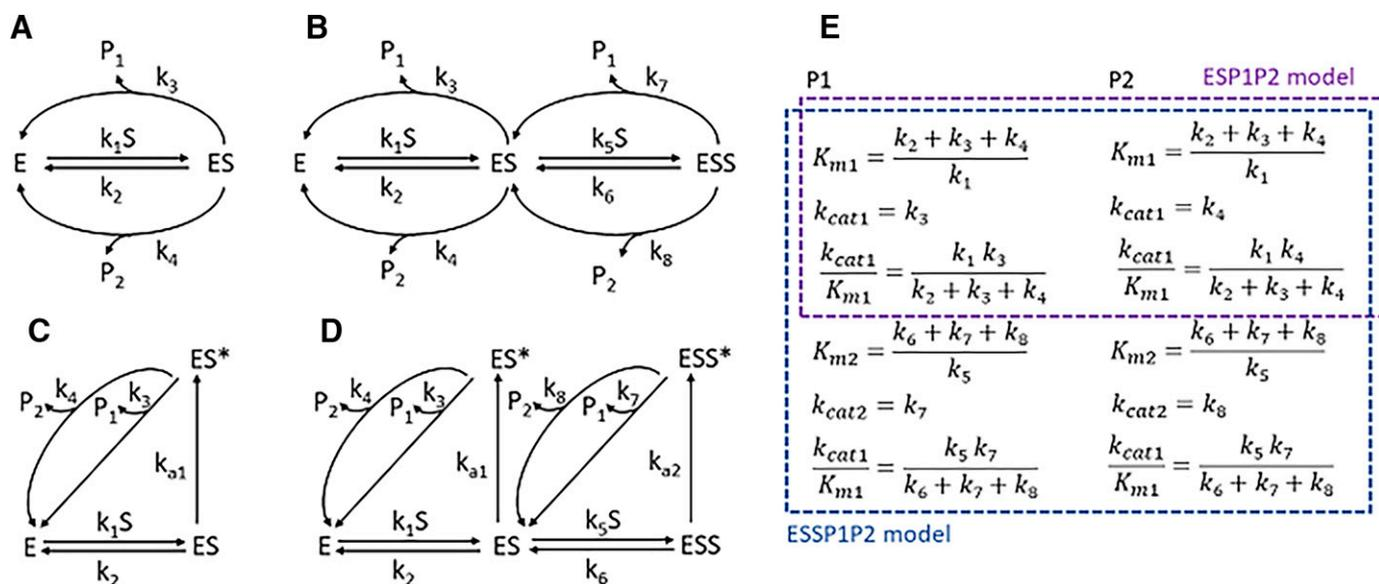


**Fig. 2.** Schemes for multiple-product formation. (A) A single-substrate binding, two-metabolite formation (ESP1P2) scheme. (B) A two-substrate binding, two-metabolite formation (ESSP1P2) scheme. (C) Single-substrate binding with rate-limiting oxygen activation. (D) Multiple-substrate binding with rate-limiting oxygen activation. (E) Expressions for  $K_m$  and  $k_{cat}$  for schemes A (dashed purple box) and B (dashed blue box) are listed. Rate constants for all reactions are denoted by  $k_1$ – $k_8$ . Rate constants  $k_{a1}$  and  $k_{a2}$  denote oxygen activation steps for  $ES^*$  and  $ESS^*$ , respectively. The species depicted in the schemes are defined as follows: E, unbound enzyme; P1, product 1; P2, product 2; and  $ES^*$  and  $ESS^*$ , active oxygen species.

### Model Fitting

For the derived velocity equation method, the Michaelis-Menten equation and ESSP rate equation (eq. 2) were fit to the simulated concentration-velocity data. The NonlinearModelFit function was used to parameterize the model with  $1/Y$  weighting.

$$\frac{velocity (v)}{E_t} = \frac{k_{cat1}S + \frac{k_{cat2}}{K_{m2}} S^2}{K_{m1} + S + \frac{S^2}{K_{m2}}} \quad (2)$$

For numerical analyses, each metabolite concentration dataset (triplicate) was used to parameterize the micro-rate constants of the ESP (one product formed from an ES model) and ESSP ODEs using NDSolve (MaxSteps  $\rightarrow$  10,000 and PrecisionGoal  $\rightarrow$   $\infty$ ) and NonlinearModelFit with  $1/Y$  weighting. Two-metabolite concentration datasets (triplicate) were used to simultaneously parameterize the micro-rate constants of the ESP1P2 (two products formed from an ES model) and ESSP1P2 ODEs.

## Results

**Two-Substrate Binding and Single-Product Formation.** Two-substrate binding can lead to atypical saturation kinetic behavior (biphasic, substrate inhibition and sigmoidal). Sigmoidal kinetics can be observed for two general scenarios:  $K_{m2} < K_{m1}$  and  $k_{cat2} > k_{cat1}$ . These general cases and the specific cases when  $k_{cat1} = 0$  are listed in Table 1, and simulations are shown in Fig. 3. Figure 3 shows simulations for four possible scenarios of sigmoidal kinetics. All of the plots in Fig. 3 show sigmoidal saturation. The impact of relative differences in kinetic parameters on the degree of sigmoidicity is also shown. When  $k_3 > 0$ , a linear range is observed at low concentrations (Fig. 3, B and C). When  $k_3 = 0$ , no linear range is observed (Fig. 3, D and E). The implication of not

having a linear range is significant. In the field of drug metabolism, a linear  $V_{max}/K_m$  describes a constant in vitro intrinsic clearance. Figure 4 shows the concentration dependence of  $CL_{int}$  for the sigmoidal kinetic curves in Fig. 3. In cases I and II, at most a 2-fold difference in  $CL_{int}$  would be observed at concentrations  $< 1 \mu M$ . It is noteworthy that up to a 100-fold difference in  $CL_{int}$  may be observed in cases III and IV.

**Two-Substrate Binding and Two-Product Formation.** Although P450s can usually form multiple metabolites, most of the kinetic models for atypical kinetics consider the dominant metabolite. Although some P450s can form more than two primary metabolites, for simplicity we have simulated the formation of two metabolites from the same P450. The scheme in Fig. 5A assumes that the formation steps for both products are rate-limiting, and P1 shows sigmoidal kinetics (Fig. 5B) since ESS formation has a higher velocity for P1 formation. Although P2 appears to have an almost hyperbolic saturation curve (Fig. 5C), the Eadie-Hofstee plot shows the kinetics are atypical. This is because there is some minimal sigmoidicity due to ESS formation even when the apparent  $K_m$  and  $k_{cat}$  for ES and ESS values are identical. Similar to Fig. 4, the higher the  $k_7/k_3$  ratio, the greater the change in P1 formation  $CL_{int}$  with increasing  $[S]$ . P2 formation  $CL_{int}$  is constant when varying  $k_7$  since substrate oxidation is not rate-limiting.

The scheme in Fig. 6A assumes that formation of active oxygenating species is rate-limiting. Again, P1 shows sigmoidal kinetics (Fig. 6B), but P2 now shows substrate inhibition (Fig. 6C). Substrate inhibition increases for P2 with increased  $k_7/k_3$  ratio.

The probability distribution of parameters to compare the use of single- versus multiple-substrate models, velocity equations versus ODEs,

TABLE 1

Different cases for sigmoidal kinetics  
The cases  $k_2 > k_5$  ( $K_{m1} > K_{m2}$ ) and  $k_6 > k_3 = 0$  ( $k_{cat1} > k_{cat2} > 0$ ) are not discussed.

Parameter	Case I	Case II	Case III	Case IV
$k_2, k_5$ ( $K_{m1}, K_{m2}$ )	$k_2 > k_5$ ( $K_{m1} > K_{m2}$ )	$k_2 = k_5$ ( $K_{m1} = K_{m2}$ )	$k_2 > k_5$ ( $K_{m1} > K_{m2}$ )	$k_2 = k_5$ ( $K_{m1} = K_{m2}$ )
$k_3, k_6$ ( $k_{cat1}, k_{cat2}$ )	$k_6 = k_3$ ( $k_{cat1} = k_{cat2} > 0$ )	$k_6 > k_3$ ( $k_{cat2} > k_{cat1} > 0$ )	$k_6 > k_3 = 0$ ( $k_{cat2} > k_{cat1} = 0$ )	$k_6 > k_3 = 0$ ( $k_{cat2} > k_{cat1} = 0$ )

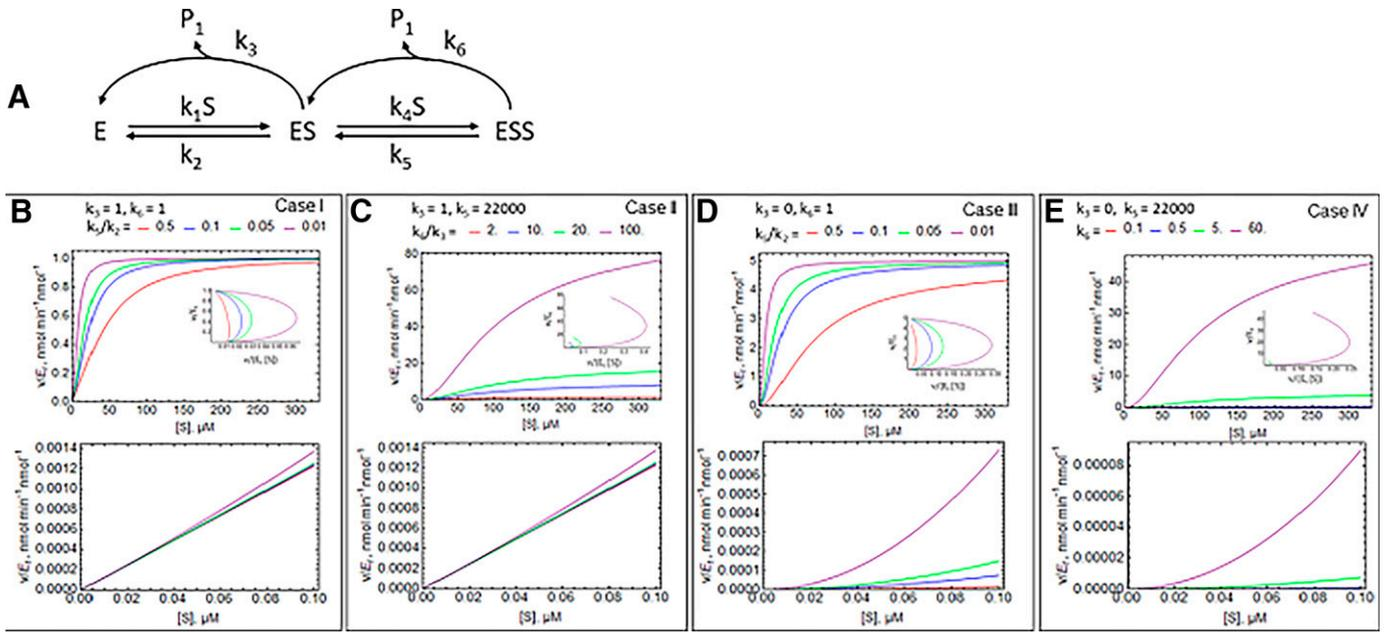


**Fig. 3.** Sigmoidal saturation curves for multiple-substrate binding and single-product formation. (A) Enzyme kinetic scheme. (B–E) Top: saturation curves (0–300  $\mu\text{M}$ ) with inset Eadie-Hofstee plots; bottom: saturation curves (0–0.1  $\mu\text{M}$ ). Common micro-rate constants:  $k_1 = k_4 = 270 \mu\text{M}^{-1}\text{min}^{-1}$ ,  $k_2 = 22,000 \text{ min}^{-1}$ . Other fixed rate constants are shown at the top of each column, and varying rate constants are at the bottom. Units for  $k_3$ ,  $k_5$ , and  $k_6$  are  $\text{min}^{-1}$ .

and single- versus multiple-product formation is shown in Fig. 7. These simulations ( $n = 500$ ) were performed using a multiple-substrate, multiple-product scheme (ESSP1P2) at error levels of 1%, 5%, and 10%. In

all cases, ESS models were necessary to accurately parameterize  $K_{m1}$  and  $k_{cat1}$ . Although the means were approximately the same for all ESS models, the distribution was narrowest for the ESS models when both

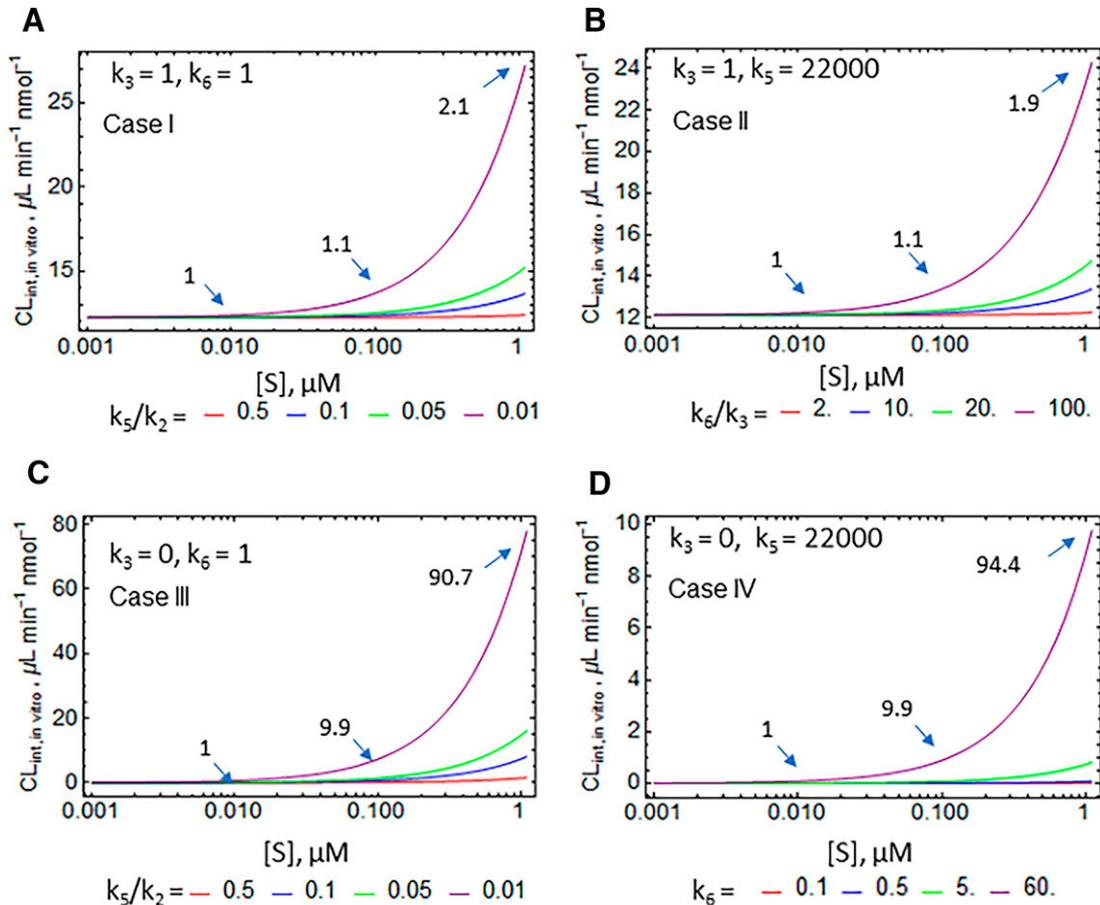


**Fig. 4.** Concentration dependence of  $CL_{int}$  for the ESS model. (A–D)  $CL_{int}$  as a function of  $[S]$  for scenarios in Table 1 and Fig. 3. The arrows indicate the fold changes in  $CL_{int}$  at 0.01, 0.1, and 1  $\mu\text{M}$ . Common micro-rate constants:  $k_1 = k_4 = 270 \mu\text{M}^{-1}\text{min}^{-1}$ ,  $k_2 = 22,000 \text{ min}^{-1}$ . Units for  $k_3$ ,  $k_5$ , and  $k_6$  are  $\text{min}^{-1}$ . Note the different scales of the y-axes.

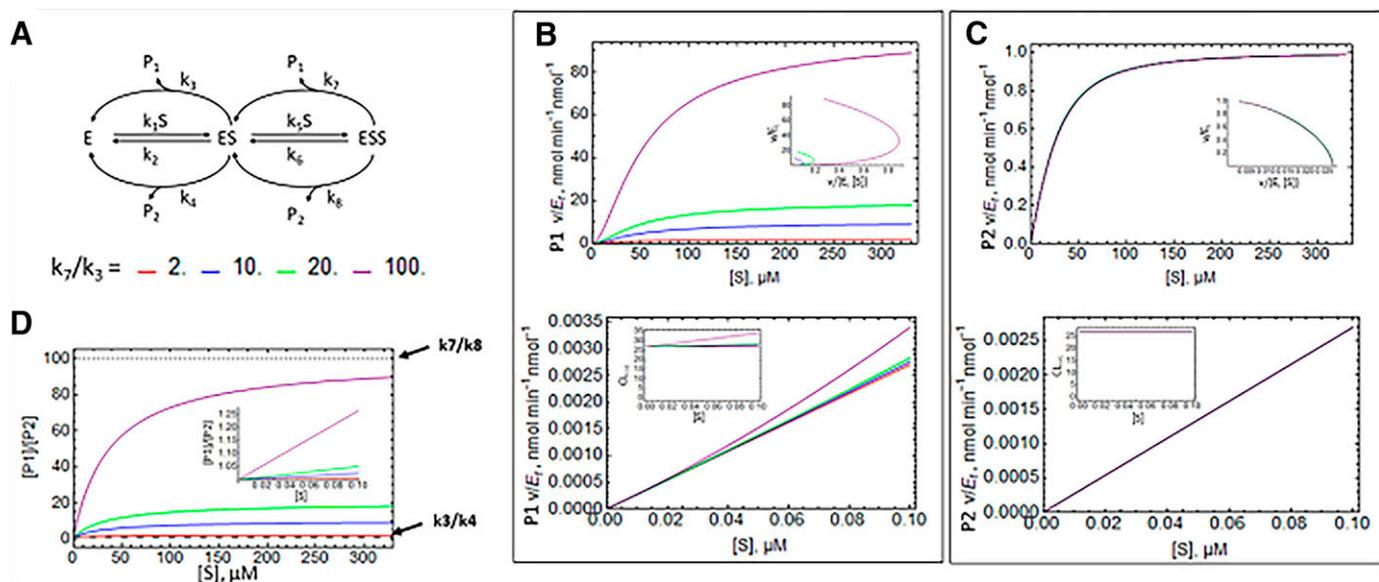


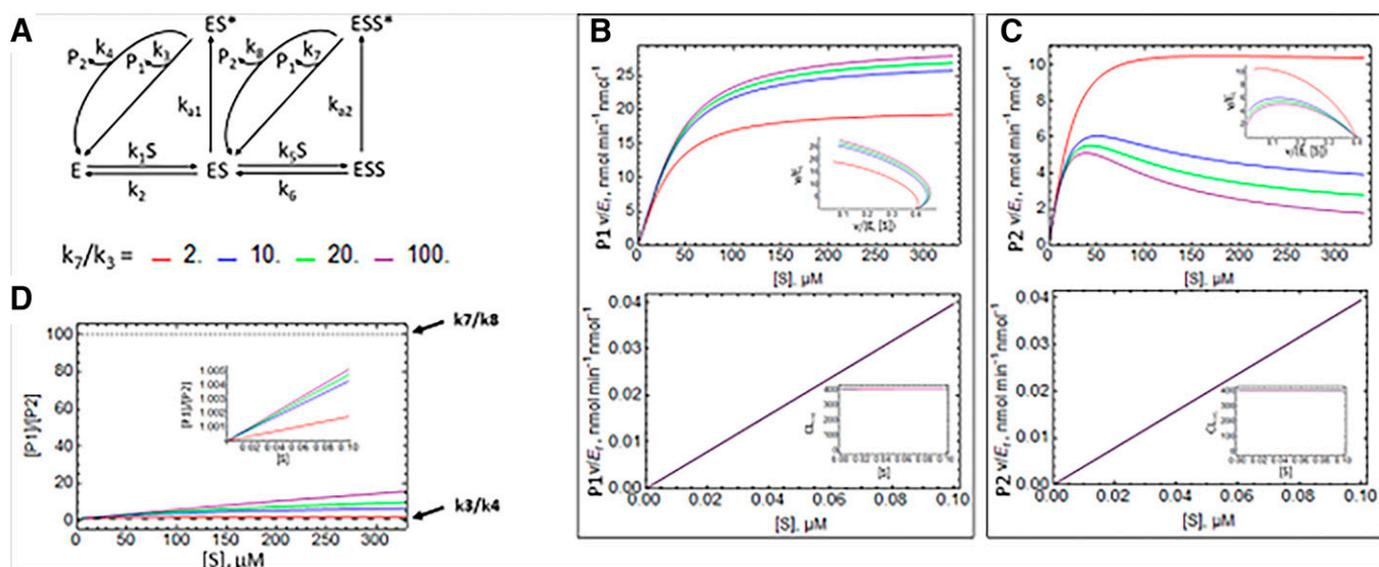
**Fig. 5.** Saturation curves for multiple-substrate binding and multiple-product formation. The scheme assumes that oxygen activation is not rate-limiting. (A) Enzyme kinetic scheme. (B and C) Top: saturation curves for P1 and P2, respectively (0–300  $\mu\text{M}$ ), with inset Eadie-Hofstee plots; bottom: saturation curves for P1 and P2, respectively (0–0.1  $\mu\text{M}$ ). (D)  $[P1]/[P2]$  metabolite ratio vs.  $[S]$ , with inset at low  $[S]$ . The dashed lines represent the  $k_3/k_4$  and  $k_7/k_8$  ratios. Fixed micro-rate constants:  $k_1 = k_5 = 270 \mu\text{M}^{-1}\text{min}^{-1}$ ,  $k_2 = k_6 = 10,000 \text{ minute}^{-1}$ ,  $k_3 = k_4 = k_8 = 1 \text{ minute}^{-1}$ .

products were modeled simultaneously. Parameters for all models tested are listed in Supplemental Table S1.

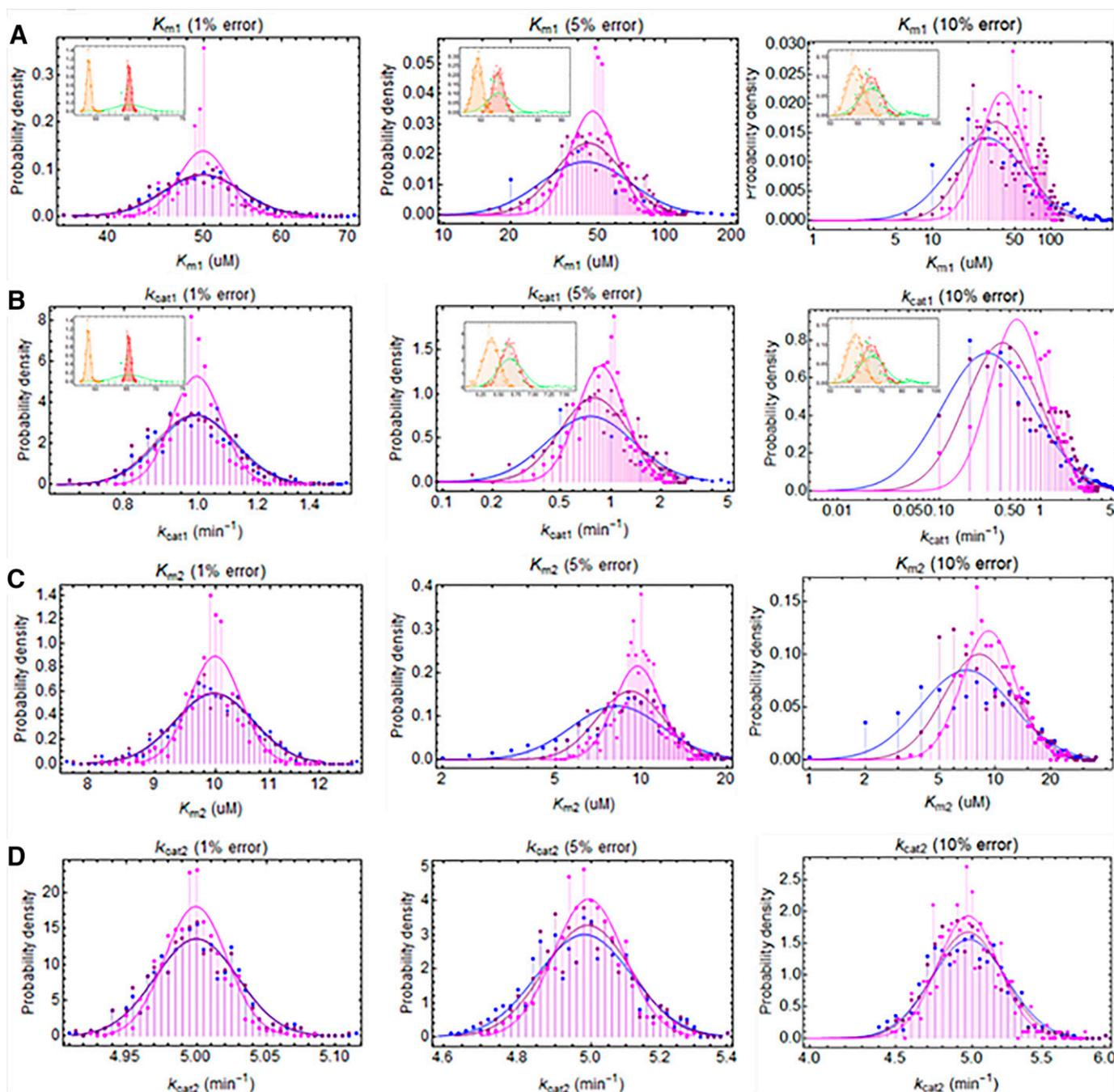
**Sequential Metabolism.** P450s can also metabolize substrates sequentially to multiple metabolites. In this section we simulated sequential metabolism using single-substrate (Fig. 8) and two-substrate binding kinetic models (Fig. 9). The kinetic scheme in Fig. 8A includes the EP1 intermediate. If P2 formation from P1 is slower than the P1 release rate, P2 will show a lag time since accumulation and rebinding of P1 to the P450 active site is necessary for P2 formation (Fig. 8B). If P2 formation from P1 is much faster than the P1 release rate, P2 will not show a lag time. Assuming linear product formation for P1, the velocities measured at different incubation times yield the same saturation curves for P1 but not with P2 (Fig. 8C).

Figure 8D shows the relationship of the rate of P1 release ( $k_5$ ) and the sequential metabolism turnover ( $k_6$ ). At  $k_6 = 27 \text{ minute}^{-1}$ , varying the ratio of  $k_5/k_6$  from 100 to 1 results in P1 dissociation constants from 10 to 0.1  $\mu\text{M}$ . Increasing the rate of P2 formation leads to a decrease in P1 formation and an increase in P2. Substrate inhibition for P2 formation becomes apparent in the Eadie-Hofstee plot since substrate competes for free enzyme with the rebinding of P1.

Sequential metabolism was also simulated with a two-substrate binding kinetic model (Fig. 9A). However, this model assumes P1 release is fast and must compete with substrate binding for free enzyme. Provided that P1 release is faster than P2 formation, these simulations should be relevant. Three types of ESS formation were simulated: when  $k_3 = k_6$ ,  $k_3 > k_6$ , and  $k_3 < k_6$  (Fig. 9, B–D, respectively). An increase in P1



**Fig. 6.** Saturation curves for multiple-substrate binding and multiple-product formation. The scheme assumes that oxygen activation is rate-limiting. (A) Enzyme kinetic scheme. (B and C) Top: saturation curves for P1 and P2, respectively (0–300  $\mu\text{M}$ ), with inset Eadie-Hofstee plots; bottom: saturation curves for P1 and P2, respectively (0–0.1  $\mu\text{M}$ ). (D)  $[P1]/[P2]$  metabolite ratio vs.  $[S]$ , with inset at low  $[S]$ . The dashed lines represent the  $k_3/k_4$  and  $k_7/k_8$  ratios. Fixed micro-rate constants:  $k_1 = k_5 = 270 \mu\text{M}^{-1}\text{min}^{-1}$ ,  $k_2 = k_6 = 10,000 \text{ minute}^{-1}$ ,  $k_3 = k_4 = k_8 = 1,000,000 \text{ minute}^{-1}$ ,  $k_{a1} = k_{a2} = 30 \text{ minute}^{-1}$ .



**Fig. 7.** The probability distribution of  $K_{m1}$ ,  $K_{m2}$ ,  $k_{cat1}$ , and  $k_{cat2}$  estimates. (A)  $K_{m1}$  at 1%, 5% and 10% error. (B)  $k_{cat1}$  at 1%, 5%, and 10% error. (C)  $K_{m2}$  at 1%, 5%, and 10% error. (D)  $k_{cat2}$  at 1%, 5%, and 10% error. The probability distribution for all parameters is depicted for the Michaelis-Menten equation (red), ESS velocity equation (blue), ES ODE (green), ESS ODE (purple), ESP1P2 ODE (orange), and ESSP1P2 ODE (magenta). Distribution is shown for 500 runs at each condition. Data were simulated with the following parameters:  $k_1 = k_5 = 270 \mu\text{M}^{-1} \text{min}^{-1}$ ,  $k_2 = 13,500 \text{min}^{-1}$ ,  $k_3 = 1 \text{min}^{-1}$ ,  $k_4 = 1 \text{min}^{-1}$ ,  $k_6 = 2700 \text{min}^{-1}$ ,  $k_7 = 5 \text{min}^{-1}$ ,  $k_8 = 1 \text{min}^{-1}$ .

affinity led to a decrease in velocity of P1 and increase in the formation of P2. As expected, P1 formation shows slight sigmoidal, substrate inhibition and sigmoidal kinetics for  $k_3 = k_6$ ,  $k_3 > k_6$ , and at  $k_3 < k_6$ , respectively. The saturation curve for P2 follows that for P1 at low [S]. At high [S], P2 formation shows substrate inhibition for all cases since increasing substrate concentrations competes with P1 rebinding.

Using numerical methods, any of the above approaches to model multiproduct and sequential metabolism can be combined. Fig. 10A shows a scheme in which two products (P1 and P2) can be formed from an ESS model, and one of the products is further metabolized to a

third product, P3. In Fig. 10B, both initial products can be metabolized to the same secondary product by sequential metabolism. For the simulations in Fig. 10C, the substrate binding constants were held constant with  $k_1$ ,  $k_5$ , and  $k_9 = 270 \mu\text{M}^{-1} \text{min}^{-1}$ ,  $k_2$  and  $k_6 = 10,000 \text{min}^{-1}$  (Rittle and Green, 2010), and the turnover rates for P1 and P2 formation were held constant with  $k_3 = 1 \text{min}^{-1}$ ,  $k_7 = 100 \text{min}^{-1}$ , and  $k_4 = k_8 = 1 \text{min}^{-1}$ . In these simulations, the dissociation constants for P1 binding were modeled at 10 and 0.1  $\mu\text{M}$ . In Fig. 10C we can see that as the affinity for P1 to the enzyme increases, P1 is rapidly converted to P3, and the ratio of P1 to P2 is decreased. As substrate

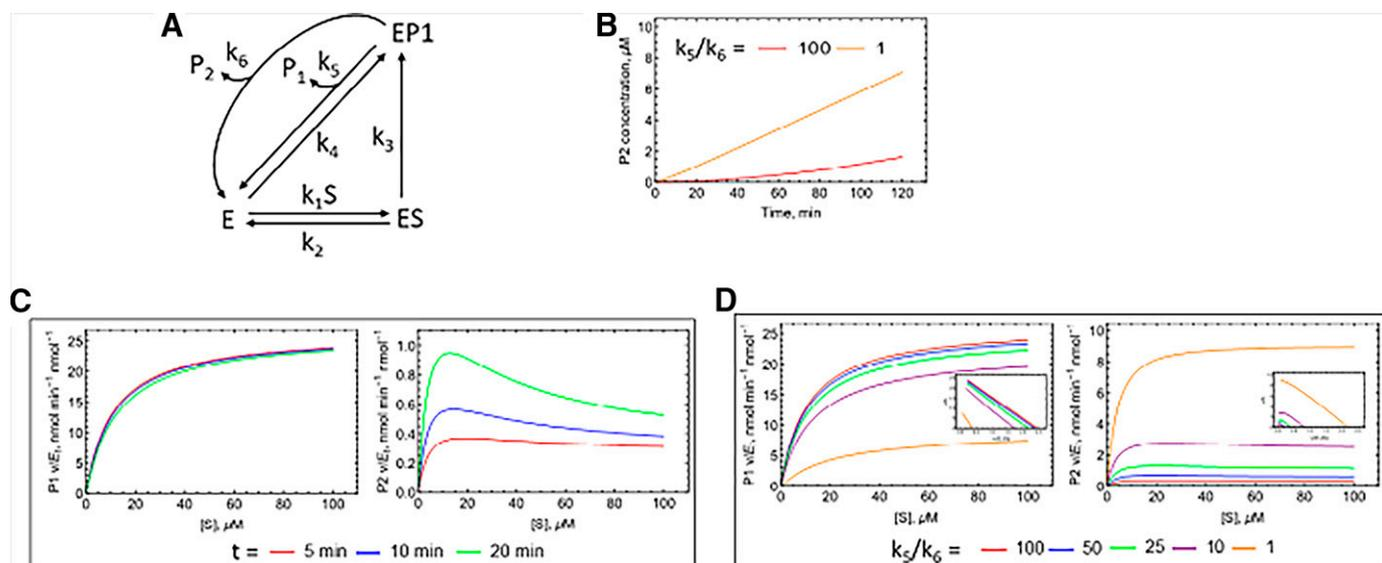


**Fig. 8.** Single-substrate binding and sequential metabolism. (A) Enzyme kinetic scheme. (B) P2 concentration over time at  $k_5/k_6 = 100$  vs. 1, exhibiting a lag time in P2 formation at  $k_5/k_6 = 100$ . (C) Saturation curve plots for P1 and P2 simulated at different incubation time ( $t$ ) at the following rate constants:  $k_1 = 270 \mu\text{M}^{-1} \text{min}^{-1}$ ;  $k_2 = 2700 \text{min}^{-1}$ ;  $k_3 = 20 \text{min}^{-1}$ ;  $k_4 = 270 \mu\text{M}^{-1} \text{min}^{-1}$ ;  $k_5 = 2700 \text{min}^{-1}$ ; and  $k_6 = 27 \text{min}^{-1}$ . (D) Saturation curve plots for products 1 and 2 simulated at different rates of product release ( $k_5$ ) and sequential metabolism turnover ( $k_6$ ). Insets: Eadie-Hofstee plots.

concentrations are increased, P1 binding is inhibited, and the expected change in P1/P2 ratios are observed. Finally, Fig. 10D shows that both the affinity and rates of sequential metabolism affect the P1/P2 ratios at different substrate concentrations.

### Discussion

The goals of this manuscript (part 1) are 4-fold: 1) to simulate and evaluate atypical kinetics using both derived velocity equations and numerical solutions using ODEs and compare the results, 2) to evaluate the impact of multiple metabolites on these models, 3) to evaluate the impact of atypical kinetics for reactions that show sequential metabolism, and 4) to provide the theoretical basis for analysis of datasets

discussed in part 2 of these manuscripts. The focus of this manuscript is on schemes and parameters that display sigmoidal saturation kinetics since these results are the most difficult to interpret.

Two standard in vitro experiments to characterize P450-mediated oxidations are saturation curves and substrate depletion assays. Substrate depletion assays observe the loss of substrate over time, usually in a microsomal incubation. This assay only requires quantitation of the substrate, a simple task since the structure is known. The assay provides an initial estimate of hepatic stability. If first-order elimination is assumed, the elimination rate constant can be used to estimate  $CL_{\text{int}}$ . This clearance value can be scaled up to a human  $CL_{\text{int}}$  using standard methods (Ito et al., 1998; Chiba et al., 2009). Once metabolites are known and standards are available, saturation curves are used to determine kinetic

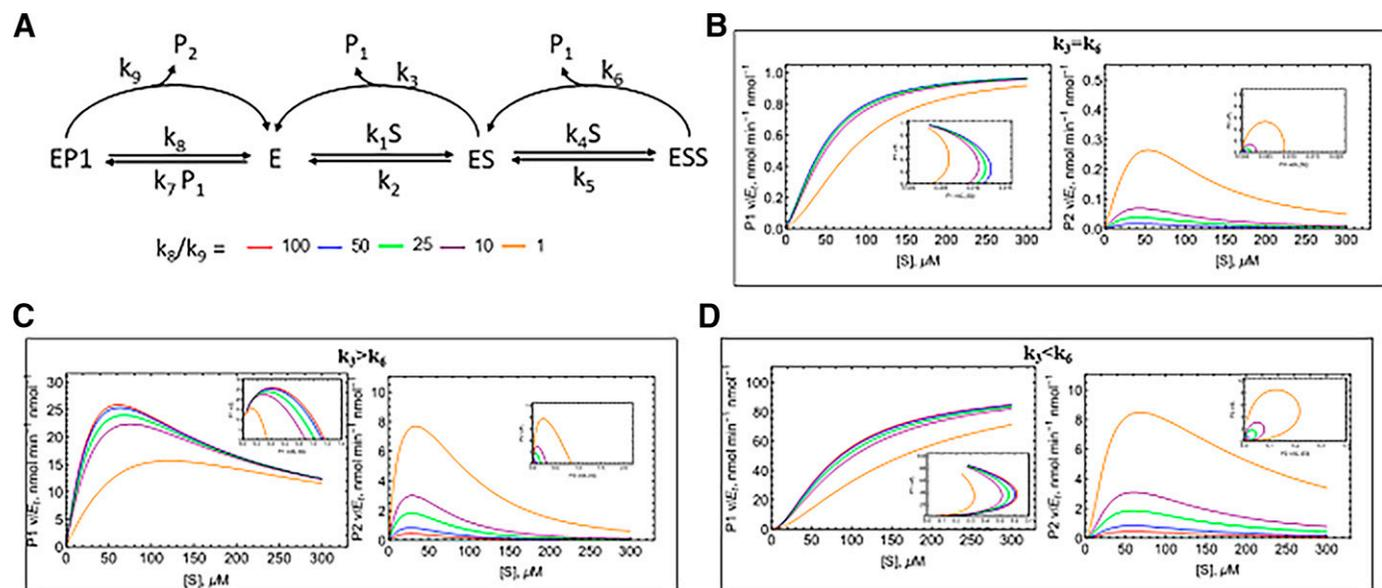


**Fig. 9.** Multiple-substrate binding and sequential metabolism. (A) Enzyme kinetic scheme. Saturation curve plots for P1 and P2 simulated at different rates of product dissociation ( $k_8$ ) and sequential metabolism turnover ( $k_9$ ), when (B)  $k_3 = k_6 = 27 \text{min}^{-1}$ . (C)  $k_3 > k_6$ ;  $k_3 = 100 \text{min}^{-1}$  and  $k_6 = 27 \text{min}^{-1}$ , and (D)  $k_3 < k_6$ ;  $k_3 = 27 \text{min}^{-1}$  and  $k_6 = 100 \text{min}^{-1}$ . Fixed values used were:  $k_1, k_4,$  and  $k_7 = 270 \mu\text{M}^{-1} \text{min}^{-1}$ ,  $k_2 = 22,000 \text{min}^{-1}$ ,  $k_5 = 11,000 \text{min}^{-1}$ ,  $k_9 = 27 \text{min}^{-1}$ . All insets depict Eadie-Hofstee plots.

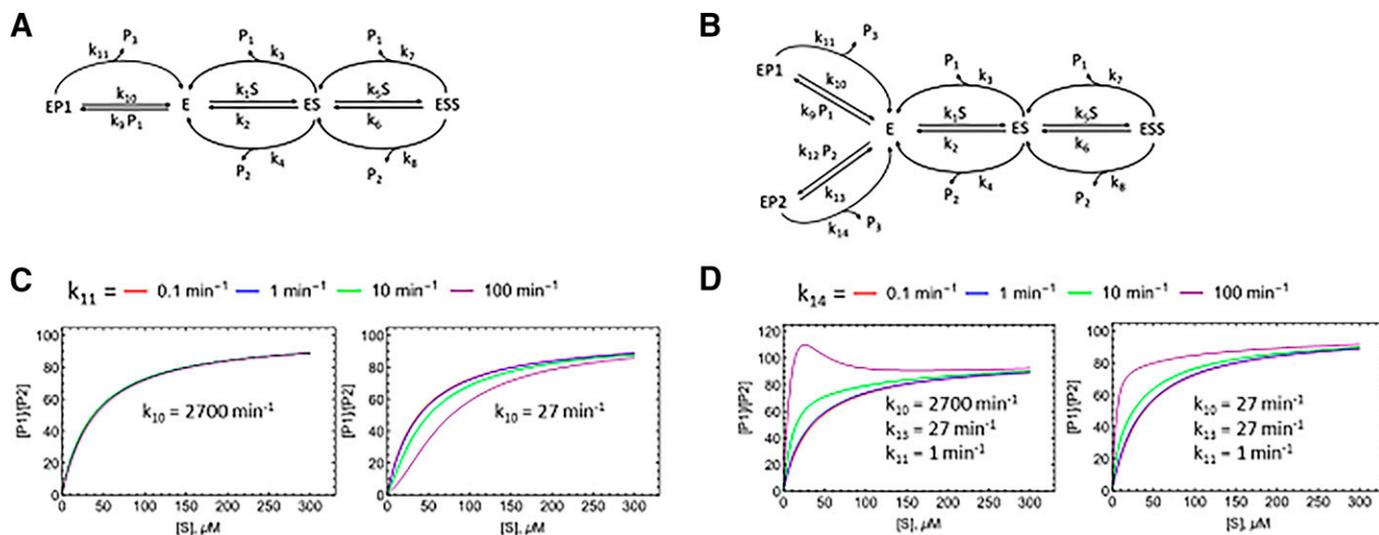


**Fig. 10.** Models for multiple-substrate binding and multiple-product formation in which (A) one or (B) two products undergo sequential metabolism. (C)  $[P1]/[P2]$  product ratio vs.  $[S]$  for model A simulated at increasing sequential turnover rate ( $k_{11}$ ) with  $k_{10}$  fixed at 2700 and 27  $\text{minute}^{-1}$ . (D)  $[P1]/[P2]$  product ratio vs.  $[S]$  for model B simulated at increasing sequential turnover rate of P2 forming P3 ( $k_{14}$ ) with  $k_{10}$  fixed at 2700 and 27  $\text{minute}^{-1}$ . Common micro-rate constants:  $k_1, k_5,$  and  $k_9 = 270 \text{ minute}^{-1}$ ,  $k_2$  and  $k_6 = 10,000 \mu\text{M}^{-1} \text{ minute}^{-1}$ ,  $k_3 = 1 \text{ minute}^{-1}$  and  $k_7 = 100 \text{ minute}^{-1}$ ,  $k_4$  and  $k_8 = 1 \text{ minute}^{-1}$ . For (D),  $k_{12} = 270 \text{ minute}^{-1}$  and  $k_{11} = 1 \text{ minute}^{-1}$ .

constants (i.e., substrate affinities and velocities). Comparing parameters for different enzymes, one can determine which P450s form which metabolites and which enzymes are likely to be important clinically. These kinetic parameters can also be used to predict whether a drug will be a victim or perpetrator of drug interactions.

Non-Michaelis-Menten kinetics are often observed for P450-mediated oxidation reactions, resulting in nonhyperbolic saturation curves, for example, sigmoidal saturation, substrate inhibition, and biphasic saturation curves (Korzekwa et al., 1998). These saturation curves are a result of multiple substrates binding simultaneously to the enzyme (e.g., Fig. 1B). Most P450-catalyzed reactions saturate well above unbound therapeutic concentrations. This results in linear pharmacokinetics since drug elimination occurs in the linear portion of the saturation curve. For substrate inhibition and biphasic saturation curves, the saturation curve is approximately linear below the  $K_m$  for ES formation. This is because the binding of the first substrate (higher affinity binding) still has a linear region at low substrate concentrations. Substrate inhibition and biphasic saturation would have to occur at very low substrate concentrations to be clinically relevant. On the other hand, sigmoidal saturation curves can be more problematic. Sigmoidal kinetics can occur when either ESS formation occurs with a higher affinity than ES formation or if  $k_{\text{cat}2}$  from ESS is faster than  $k_{\text{cat}1}$  from ES (e.g.,  $k_6 > k_3$  in Fig. 1B). If  $k_{\text{cat}1}$  contributes substantially at therapeutic concentrations, there may still be a linear region. However, if  $k_{\text{cat}1}$  approaches zero, there may not be a linear region at low substrate concentrations. This will result in a different estimate of intrinsic clearance for different initial substrate concentrations (e.g., see Fig. 4). An example of the impact of using an Michaelis-Menten model to predict the intrinsic clearance of an enzyme showing sigmoidal kinetics is shown in part 2 of these manuscripts.

The results in Fig. 3 are as expected, with the sigmoidal saturation curves having a linear region at low substrate concentrations when  $k_{\text{cat}1}$  ( $k_3$ ) is  $>0$  (Fig. 3, B and C) and no linear region when  $k_3 = 0$  (Fig. 3, D and E). All simulations give the expected Eadie-Hofstee plots showing convex curvature to the right. Figure 4 shows the impact of low  $k_{\text{cat}1}$  values on  $CL_{\text{int}}$ . When  $k_{\text{cat}1}$  is 1, sigmoidicity due to either higher affinity binding of the second substrate or higher velocity of the second substrate results in modest increases in  $CL_{\text{int}}$  ( $\sim 2$ -fold between 10 nM and 1  $\mu\text{M}$  for 100-fold increases in affinity or velocity for ESS; Fig. 4,

A and B). However, when  $k_{\text{cat}1} = 0$ ,  $\sim 100$ -fold increases in  $CL_{\text{int}}$  are observed for  $[S]$  between 10 nM and 1  $\mu\text{M}$  (Fig. 4, C and D). Also, there is no range in which  $CL_{\text{int}}$  is constant. An  $\sim 100$ -fold increase in  $CL_{\text{int}}$  would be observed for  $[S]$  between 0.1 nM and 10 nM as well. This nonlinearity can be identified with substrate depletion assays at different substrate concentrations. Predicting in vivo  $CL_{\text{int}}$  would require conducting in vitro assays at  $[S]$  that match the unbound intracellular concentrations. Also, concentration-dependent  $CL_{\text{int}}$  in vitro may result in nonlinear pharmacokinetics in vivo.

Sequential metabolism by the P450s is important in drug discovery and development since metabolites can be active or toxic or cause drug-drug interactions (Jackson et al., 2018; Wienkers and Rock, 2021). We have simulated P450 kinetic models that can form two different products from either a single-substrate complex (Fig. 2, A and C) or from an ESS complex (Fig. 2, B and D). These models do not include both multiple-product formation and sequential metabolism. If a substrate can only bind once (Fig. 2, A and C) the P1/P2 product ratio remains constant at  $k_3/k_4$ . However, for multisubstrate kinetics, metabolite ratios can change with substrate concentrations. Figure 5 is the simplest scheme for two products formed from ES and ESS complexes. The simulations in Fig. 5 show increasing formation of P1 from ESS while holding all other parameters constant. As expected, P1 formation shows increasing sigmoidicity as  $k_7$  increases because of the higher velocity for P1 formation from ESS. However, this scheme does not accurately capture the impact of increasing one product formation pathway for a P450 reaction. As shown in Fig. 5C, changing  $k_7$  has no impact on P2 formation. This is because binding is fast, and the rate-limiting steps in this scheme are the product formation steps ( $k_3, k_4, k_7,$  and  $k_8$ ). In reality, the rate-limiting step for P450 oxidations is the formation of an active oxygenating species, and this active oxygenating species can form different metabolites. This results in the P450 property called “metabolic switching” wherein blocking one site results in increased metabolism at other sites. This can be best modeled using the schemes in Fig. 2, C and D and Fig. 6. In Fig. 6C, increasing  $k_7$  while holding all parameters constant results in a decrease in P2 formation at high substrate concentrations. Since formation of the active oxygenating species is rate-limiting, increasing P1 formation must result in a decrease in P2 formation. For a chemist modifying a molecule for stability, the

difference between the schemes in Figs. 5 and 6 is important since decreasing metabolism at one position may increase metabolism at another. However, when fitting kinetic models to experimental datasets for multiple products, the simpler scheme in Fig. 5 is preferred. The same substrate inhibition profile for P2 seen in Fig. 6C would also be observed if  $k_8 < k_4$ . Using the method of Cleland (1975) and the scheme in Fig. 6, net rate constants can be calculated for conversion of ES and ESS complexes to products, and the result is the simplified scheme in Fig. 5. For example, the net rate constant for P1 formation from ES in Fig. 6 ( $k_{a1} k_3 / (k_3 + k_4)$ ) will be equal to  $k_3$  in Fig. 5.

The parameter probability distributions for the various simulations shown in Fig. 7 show that 1) using an ES model for ESS kinetics results in inaccurate  $K_m$  and  $k_{cat}$  values, 2) use of ODEs instead of derived velocity equations minimizes the overall parameter errors, and 3) simultaneous fitting to both P1 and P2 data further decreases the parameter errors. These results suggest that using ODEs to model P450 kinetics is generally preferred to using derived velocity equations. Derived velocity equations include additional simplifying assumptions, and equations for complex systems these equations are generally not available.

When sequential metabolism occurs, the rate of the first product release (P1 in Fig. 8A) has a large impact on the kinetics of the sequential product (P2). If P1 release is fast, there will be a lag time for P2 formation since P1 must accumulate before P2 can be formed. Also, P2 formation can be inhibited by high substrate concentrations. Lag times have frequently been observed for time-dependent inhibition kinetics when multiple oxidation steps are required for P450 inactivation. Figure 9 considers a scenario that includes multiple-substrate binding and sequential metabolism with mandatory P1 release. A complete model would additionally include ESP1, ESP2, EP1P1, EP1P2, and EP2P2. Limiting schemes to mandatory product release may not always be sufficient to model experimental data (see part 2). Finally, schemes can be readily constructed for multiple-substrate binding with multiple-product formation as well sequential metabolism (Fig. 10). Adding sequential metabolism can result in unusual P1/P2 product ratio curves when one or both products are further metabolized. A wide range of product ratio curves is possible for a variety of schemes and kinetic scenarios (e.g., see Fig. 10D). When experimental data are available for both P1 and P2 formation, product ratio plots can be very useful in selecting appropriate kinetic schemes (see part 2).

Mechanisms can vary for different substrates with the same P450 and for different P450s with the same substrate. The diversity of possible mechanisms requires that statistical methods be used to determine the best model for a given dataset. We use corrected Akaike information criterion values to compare different mechanisms since this method can be used for nested and non-nested models. It is also important to plot residuals. A run of signs indicates that the model is likely inadequate and may bias data interpretation. Parameter errors should be compared with the parameter estimates since covariance will result in large relative parameter errors. This can also be observed in the correlation matrix for the calculation. It should be noted that insufficient data and high experimental errors can result in inaccurate model selection.

Finally, in part 2 of these manuscripts, we have used numerical methods to simultaneously model the multiple metabolites formed initially and sequentially from diazepam by CYP3A4. This resulted in a mechanistic interpretation of diazepam metabolism that provided affinities and velocities consistent with the observed metabolic data for diazepam and its metabolites.

In conclusion, we have modeled combinations of multiple-substrate binding, multiple-product formation, and sequential metabolism. We have focused on sigmoidal kinetics since they can have a dramatic impact on clearance predictions. The use of Michaelis-Menten models to characterize multisubstrate saturation data results in inaccurate kinetic

parameters and clearance predictions. Comparing results for use of standard velocity equations with ODEs clearly shows that ODEs are more versatile and provide better parameter estimates. The complexity of the kinetic schemes used for these analyses shows that most kinetic schemes can be modeled, and these models can be parameterized provided that sufficient experimental data are available. Finally, these analyses provide a framework for modeling the experimental P450 kinetics observed in part 2 of these manuscripts.

#### Authorship Contributions

*Participated in research design:* Wang, Paragas, Korzekwa.  
*Conducted experiments:* Wang, Paragas.  
*Performed data analysis:* Wang, Paragas, Nagar, Korzekwa.  
*Wrote or contributed to the writing of the manuscript:* Wang, Paragas, Nagar, Korzekwa.

#### References

- Atkins WM (2005) Non-Michaelis-Menten kinetics in cytochrome P450-catalyzed reactions. *Annu Rev Pharmacol Toxicol* **45**:291–310.
- Atkins WM (2006) Current views on the fundamental mechanisms of cytochrome P450 allosterism. *Expert Opin Drug Metab Toxicol* **2**:573–579.
- Barnaba C, Yadav J, Nagar S, Korzekwa K, and Jones JP (2016) Mechanism-based inhibition of CYP3A4 by podophyllotoxin: aging of an intermediate is important for in vitro/in vivo correlations. *Mol Pharm* **13**:2833–2843.
- Blobaum AL, Bridges TM, Byers FW, Turlington ML, Mattmann ME, Morrison RD, Mackie C, Lavreysen H, Bartolomé JM, Macdonald GJ, et al. (2013) Heterotropic activation of the midazolam hydroxylase activity of CYP3A by a positive allosteric modulator of mGlu5: in vitro to in vivo translation and potential impact on clinically relevant drug-drug interactions. *Drug Metab Dispos* **41**:2066–2075.
- Chiba M, Ishii Y, and Sugiyama Y (2009) Prediction of hepatic clearance in human from in vitro data for successful drug development. *AAPS J* **11**:262–276.
- Cleland WW (1975) Partition analysis and the concept of net rate constants as tools in enzyme kinetics. *Biochemistry* **14**:3220–3224.
- Cleland WW (1979) Statistical analysis of enzyme kinetic data. *Methods Enzymol* **63**:103–138.
- Collom SL, Laddusaw RM, Burch AM, Kuzmic P, Perry Jr MD, and Miller GP (2008) CYP2E1 substrate inhibition. Mechanistic interpretation through an effector site for monocyclic compounds. *J Biol Chem* **283**:3487–3496.
- Dangi B, Davydova NY, Maldonado MA, Ahire D, Prasad B, and Davydov DR (2021) Probing functional interactions between cytochromes P450 with principal component analysis of substrate saturation profiles and targeted proteomics. *Arch Biochem Biophys* **708**:108937.
- Davydov DR, Davydova NY, Rodgers JT, Rushmore TH, and Jones JP (2017) Toward a systems approach to the human cytochrome P450 ensemble: interactions between CYP2D6 and CYP2E1 and their functional consequences. *Biochem J* **474**:3523–3542.
- Domanski TL, He YA, Khan KK, Roussel F, Wang Q, and Halpert JR (2001) Phenylalanine and tryptophan scanning mutagenesis of CYP3A4 substrate recognition site residues and effect on substrate oxidation and cooperativity. *Biochemistry* **40**:10150–10160.
- Ekins S, Stresser DM, and Williams JA (2003) In vitro and pharmacophore insights into CYP3A enzymes. *Trends Pharmacol Sci* **24**:161–166.
- Ekroos M and Sjögren T (2006) Structural basis for ligand promiscuity in cytochrome P450 3A4. *Proc Natl Acad Sci USA* **103**:13682–13687.
- Frenzen CL and Maini PK (1988) Enzyme kinetics for a two-step enzymic reaction with comparable initial enzyme-substrate ratios. *J Math Biol* **26**:689–703.
- Galetin A, Brown C, Hallifax D, Ito K, and Houston JB (2004) Utility of recombinant enzyme kinetics in prediction of human clearance: impact of variability, CYP3A5, and CYP2C19 on CYP3A4 probe substrates. *Drug Metab Dispos* **32**:1411–1420.
- Galetin A, Clarke SE, and Houston JB (2003) Multisite kinetic analysis of interactions between prototypical CYP3A4 subgroup substrates: midazolam, testosterone, and nifedipine. *Drug Metab Dispos* **31**:1108–1116.
- Gay SC, Roberts AG, and Halpert JR (2010) Structural features of cytochromes P450 and ligands that affect drug metabolism as revealed by X-ray crystallography and NMR. *Future Med Chem* **2**:1451–1468.
- Guengerich FP (2018) Mechanisms of cytochrome P450-catalyzed oxidations. *ACS Catal* **8**:10964–10976.
- Hemker P (1972) Numerical methods for differential equations in system simulation and in parameter estimation. *Analysis and Simulation of biochemical systems* **28**:59–80.
- Hosea NA, Miller GP, and Guengerich FP (2000) Elucidation of distinct ligand binding sites for cytochrome P450 3A4. *Biochemistry* **39**:5929–5939.
- Hutzler JM and Tracy TS (2002) Atypical kinetic profiles in drug metabolism reactions. *Drug Metab Dispos* **30**:355–362.
- Ito K, Iwatsubo T, Kanamitsu S, Nakajima Y, and Sugiyama Y (1998) Quantitative prediction of in vivo drug clearance and drug interactions from in vitro data on metabolism, together with binding and transport. *Annu Rev Pharmacol Toxicol* **38**:461–499.
- Iwaki M, Niwa T, Tanaka H, Kawase A, and Komura H (2019) Prediction of hepatic clearance of stereoselective metabolism of carvedilol in liver microsomes and hepatocytes of Sprague-Dawley and cytochrome P450 2D-deficient dark Agouti rats. *J Pharm Pharm Sci* **22**:72–84.
- Jackson KD, Durandis R, and Vergne MJ (2018) Role of cytochrome P450 enzymes in the metabolic activation of tyrosine kinase inhibitors. *Int J Mol Sci* **19**:2367.
- Jamakhandi AP, Kuzmic P, Sanders DE, and Miller GP (2007) Global analysis of protein-protein interactions reveals multiple CYP2E1-reductase complexes. *Biochemistry* **46**:10192–10201.
- Johnson KA (2009) Fitting enzyme kinetic data with KinTek Global Kinetic Explorer. *Methods Enzymol* **467**:601–626.

- Jones JP and Korzekwa KR (1996) Predicting the rates and regioselectivity of reactions mediated by the P450 superfamily. *Methods Enzymol* **272**:326–335.
- Kenworthy KE, Clarke SE, Andrews J, and Houston JB (2001) Multisite kinetic models for CYP3A4: simultaneous activation and inhibition of diazepam and testosterone metabolism. *Drug Metab Dispos* **29**:1644–1651.
- Komura H, Kawase A, and Iwaki M (2005) Application of substrate depletion assay for early prediction of nonlinear pharmacokinetics in drug discovery: assessment of nonlinearity of metoprolol, timolol, and propranolol. *J Pharm Sci* **94**:2656–2666.
- Korzekwa K (2021) Enzyme kinetics of oxidative metabolism-cytochromes P450. *Methods Mol Biol* **2342**:237–256.
- Korzekwa K, Tweedie D, Argikar UA, Whitcher-Johnstone A, Bell L, Bickford S, and Nagar S (2014) A numerical method for analysis of in vitro time-dependent inhibition data. Part 2. Application to experimental data. *Drug Metab Dispos* **42**:1587–1595.
- Korzekwa KR, Krishnamachary N, Shou M, Ogai A, Parise RA, Rettie AE, Gonzalez FJ, and Tracy TS (1998) Evaluation of atypical cytochrome P450 kinetics with two-substrate models: evidence that multiple substrates can simultaneously bind to cytochrome P450 active sites. *Biochemistry* **37**:4137–4147.
- Kuzmič P (2009) DynaFit—a software package for enzymology. *Methods Enzymol* **467**:247–280.
- Li H and Poulos TL (2004) Crystallization of cytochromes P450 and substrate-enzyme interactions. *Curr Top Med Chem* **4**:1789–1802.
- Luthra A, Denisov IG, and Sligar SG (2011) Spectroscopic features of cytochrome P450 reaction intermediates. *Arch Biochem Biophys* **507**:26–35.
- Manimozhi P, Subbiah A, and Rajendran L (2010) Solution of steady-state substrate concentration in the action of biosensor response at mixed enzyme kinetics. *Sens Actuators B Chem* **147**:290–297.
- Masubuchi Y, Iwasa T, Fujita S, Suzuki T, Horie T, and Narimatsu S (1996) Regioselectivity and substrate concentration-dependency of involvement of the CYP2D subfamily in oxidative metabolism of amitriptyline and nortriptyline in rat liver microsomes. *J Pharm Pharmacol* **48**:925–929.
- Michaelis L and Menten ML (1913) Die kinetik der invertinwirkung. *Biochem Z* **49**:352.
- Nagar S, Jones JP, and Korzekwa K (2014) A numerical method for analysis of in vitro time-dependent inhibition data. Part 1. Theoretical considerations. *Drug Metab Dispos* **42**:1575–1586.
- Nguyen HQ, Kimoto E, Callegari E, and Obach RS (2016) Mechanistic modeling to predict midazolam metabolite exposure from in vitro data. *Drug Metab Dispos* **44**:781–791.
- Obach RS (2013) Pharmacologically active drug metabolites: impact on drug discovery and pharmacotherapy. *Pharmacol Rev* **65**:578–640.
- Pang KS (1995) Kinetics of sequential metabolism. Contribution of parallel, primary metabolic pathways to the formation of a common, secondary metabolite. *Drug Metab Dispos* **23**:166–177.
- Plant RE (1979) The efficient numerical solution of biological simulation problems. *Comput Programs Biomed* **10**:1–15.
- Rajendran L, Devi MC, Fernandez C, and Peng Q (2018) *Mathematical Modeling and Simulation of Nonlinear Process in Enzyme Kinetics*. InTech, London.
- Rittle J and Green MT (2010) Cytochrome P450 compound I: capture, characterization, and C-H bond activation kinetics. *Science* **330**:933–937.
- Roberts AG, Yang J, Halpert JR, Nelson SD, Thummel KT, and Atkins WM (2011) The structural basis for homotropic and heterotropic cooperativity of midazolam metabolism by human cytochrome P450 3A4. *Biochemistry* **50**:10804–10818.
- Schadt S, Bister B, Chowdhury SK, Funk C, Hop CECA, Humphreys WG, Igarashi F, James AD, Kagan M, Khojasteh SC, et al. (2018) A decade in the MIST: Learnings from investigations of drug metabolites in drug development under the “Metabolites in Safety Testing” regulatory guidance. *Drug Metab Dispos* **46**:865–878.
- Sevrioukova IF and Poulos TL (2017) Structural basis for regiospecific midazolam oxidation by human cytochrome P450 3A4. *Proc Natl Acad Sci USA* **114**:486–491.
- Shou M, Grogan J, Mancewicz JA, Krausz KW, Gonzalez FJ, Gelboin HV, and Korzekwa KR (1994) Activation of CYP3A4: evidence for the simultaneous binding of two substrates in a cytochrome P450 active site. *Biochemistry* **33**:6450–6455.
- Tracy TS (2006) Atypical cytochrome p450 kinetics: implications for drug discovery. *Drugs R D* **7**:349–363.
- Ueng Y-F, Kuwabara T, Chun Y-J, and Guengerich FP (1997) Cooperativity in oxidations catalyzed by cytochrome P450 3A4. *Biochemistry* **36**:370–381.
- Varón R, Havsteen BH, Valero E, Molina-Alarcón M, García-Cánovas F, and García-Moreno M (2005) Kinetic analysis of the transient phase and steady state of open multicyclic enzyme cascades. *Acta Biochim Pol* **52**:765–780.
- Walsky RL and Obach RS (2004) Validated assays for human cytochrome P450 activities. *Drug Metab Dispos* **32**:647–660.
- Wester MR, Yano JK, Schoch GA, Yang C, Griffin KJ, Stout CD, Johnson EF, White CR, and Seymour RS (2005) The structure of human cytochrome P450C9 complexed with flurbiprofen at 2.0-angstrom resolution allometric scaling of mammalian metabolism. *J Exp Biol* **208**:35630–35637.
- Wienkers LC and Rock BM (2021) Multienzyme kinetics and sequential metabolism. *Methods Mol Biol* **2342**:89–112.
- Yadav J, Korzekwa K, and Nagar S (2018) Improved predictions of drug-drug interactions mediated by time-dependent inhibition of CYP3A. *Mol Pharm* **15**:1979–1995.
- Yadav J, Korzekwa K, and Nagar S (2021) Numerical methods for modeling enzyme kinetics. *Methods Mol Biol* **2342**:147–168.
- Yadav J, Paragas E, Korzekwa K, and Nagar S (2020) Time-dependent enzyme inactivation: numerical analyses of in vitro data and prediction of drug-drug interactions. *Pharmacol Ther* **206**:107449.
- Yano JK, Wester MR, Schoch GA, Griffin KJ, Stout CD, and Johnson EF (2004) The structure of human microsomal cytochrome P450 3A4 determined by X-ray crystallography to 2.05-Å resolution. *J Biol Chem* **279**:38091–38094.
- Yoon MY, Campbell AP, and Atkins WM (2004) “Allosterism” in the elementary steps of the cytochrome P450 reaction cycle. *Drug Metab Rev* **36**:219–230.
- Zanger UM and Schwab M (2013) Cytochrome P450 enzymes in drug metabolism: regulation of gene expression, enzyme activities, and impact of genetic variation. *Pharmacol Ther* **138**:103–141.

**Address correspondence to:** Dr. Ken Korzekwa, 3307 N. Broad St., Philadelphia, PA 19140. E-mail: korzekwa@temple.edu